Self-trapping of excitations: Two-dimensional quasiparticle solitons in an extended Bose-Hubbard dimer array

Amit Dey and Amichay Vardi
Department of Chemistry, Ben-Gurion University of the Negev, Beer-Sheva 84105, Israel
(Received 18 December 2016; published 27 March 2017)

Considering a two-dimensional (2D) Bose-Hubbard spinor lattice with weak nearest-neighbor interactions and no particle transfer between sites, we theoretically study the transport of energy from one initially excited dimer to the rest of the lattice. Beyond a critical interaction strength, low-energy on-site excitations are quickly dispersed throughout the array, while stronger excitations are self-trapped, resulting in localized energy breathers and solitons. These structures are quasiparticle analogs to the discrete 2D solitons in photonic lattices. Full many-body simulations additionally demonstrate the localization of one-particle entropy.

DOI: 10.1103/PhysRevA.95.033630

I. INTRODUCTION

Depending upon the competing interaction scales, the dynamics of bosonic Josephson junctions (BJJs) composed of two coupled Bose-Einstein condensates (BECs) give rise to intriguing phenomena such as Josephson oscillation [1,2] and macroscopic quantum self-trapping [3–6]. The first phenomenon is a signature of macroscopic phase coherence already realized in superconductor Josephson junctions and in superfluid helium [7], whereas the second emerges as a consequence of interactions among the condensate particles. Weak nonlinear interparticle interaction results in anharmonic Josephson oscillations between the two condensates. When the interaction is sufficiently strong, a new dynamical self-trapping regime appears [4,5]. Thus, while low population imbalance preparation still gives full population oscillations between the condensates, larger initial population differences remain self-trapped.

This BJJ dynamics is captured well by a tight-binding two-mode Bose-Hubbard Hamiltonian (BHH) [1,8–10]. The BHH model has one characteristic interaction parameter $u \equiv UN/K$, with U, N, and K being the interaction strength, the total number of atoms, and the hopping frequency, respectively. In the classical, mean-field limit, when $u > 1$, the $\{n,\varphi\}$ phase space, where n and φ are the population imbalance and relative phase between the modes, is split by a separatrix trajectory into a Josephson oscillation region and a self-trapping region [1,9,11,12]. If $n(t = 0)$ is above the separatrix, one obtains self-trapping. Similar self-trapped solutions can be found for attractive interaction ($u < -1$) with the same population imbalance and an opposite phase.

Going beyond a single BJJ, a system of two coupled Bose-Hubbard (BH) dimers was considered in Refs. [13–18]. The low-energy dynamics of this configuration was shown to involve two Josephson modes in which both particles and elementary Bogoliubov excitations (termed "josons" in Ref. [13]) are transferred between the dimers. The nonlinear repulsive interaction between the atoms was shown to result in an attraction between these quasiparticles. In a two-dimensional array of weakly coupled BH dimers, the joson attraction leads to their spontaneous accumulation which, on identification of excitations as "heat", emulates negative specific heat in cold-atom systems [19].

Since the possibility to transfer excitation energy as well as particles opens the way for a second Josephson oscillation mode, it is natural to ask whether excitation energy can also be self-trapped. Here, we explore this possibility using an extended Bose-Hubbard dimer array model. We consider N particles in a two-dimensional $M \times M$ array of spinor BECs, [20] where each site has two internal degrees of freedom. To focus on the dynamics of excitations rather than on the transport of particles, there is no particle transfer between the dimers, yet energy transfer is allowed via weak interaction between particles in adjacent sites. This extended Bose-Hubbard model corresponds to the tight-binding description of BECs of particles with permanent magnetic or electric dipole moments, confined by periodic potentials [21].

Launching the system with one excited site, whereas all other sites are in their respective ground states, we study the transport of the excitation energy within the array. For sufficiently strong interaction, excitations beyond a critical energy are self-trapped, resulting in energy breathers and solitons, while weaker on-site excitations are rapidly dispersed throughout the array. These excitation solitons are analogous to the two-dimensional discrete solitons obtained in photonic lattices [22] and suggested for BECs in optical lattices [23]. However, in our case quasiparticles (namely Josephson excitations) are localized instead of particles. This leads to the localization of one-particle entropy as well as of energy, distinguishing the new structures as "heat solitons".

The rest of the paper is arranged as follows. In Sec. II we introduce the extended Bose-Hubbard Hamiltonian and the many-body quantum treatment is outlined in Sec. III. In Sec. IV we derive the classical mean-field equations of motion. Section V describes the equivalent Hamiltonian in the excitation basis and explains the critical nature of excitation trapping. In Sec. VI we present both classical and quantum simulation results for the case when only a single site is initially excited, whereas in Sec. VII the case for an initially excited block of sites is dealt with. Finally, conclusions are provided in Sec. VIII.

II. MODEL HAMILTONIAN

The extended BHH for our system reads

$$H = H_0 + H_c, \tag{1}$$

 ©2017 American Physical Society

where the uncoupled dimer Hamiltonian H_0 and the coupling Hamiltonian H_c are given by

$$H_0 = \sum_i \left[-\frac{K}{2}(\hat{a}_i^\dagger \hat{b}_i + \hat{b}_i^\dagger \hat{a}_i) + \frac{U}{2}\left(\hat{n}_{a,i}^2 + \hat{n}_{b,i}^2\right) \right] \quad (2)$$

and

$$H_c = \frac{\mathcal{U}_{aa}}{2} \sum_{\langle i,j \rangle} (\hat{n}_{a,i}\hat{n}_{a,j} + \hat{n}_{b,i}\hat{n}_{b,j}) + \frac{\mathcal{U}_{ab}}{2} \sum_{\langle i,j \rangle} (\hat{n}_{a,i}\hat{n}_{b,j} + \hat{n}_{b,i}\hat{n}_{a,j}), \quad (3)$$

respectively. In the above, $\hat{a}_i$ and $\hat{b}_i$ are the bosonic destruction operators for the two dimer modes at site $i \equiv \{i_1, i_2\}$ and the respective mode populations are $\hat{n}_{a,i} = \hat{a}_i^\dagger \hat{a}_i$, $\hat{n}_{b,i} = \hat{b}_i^\dagger \hat{b}_i$. The intradimer coupling strength between the two modes and the on-site interparticle interaction strength are given by K and U, whereas $\mathcal{U}_{aa}$ and $\mathcal{U}_{ab}$ are same-mode and opposite-mode nearest-neighbor interaction strengths, respectively. We choose parameter values $K, U \gg \mathcal{U}_{aa}, \mathcal{U}_{ab}$ to have time-scale separation between the fast intradimer and slow interdimer dynamics. Since no intersite particle transfer is allowed, particle numbers $n_i = n_{a,i} + n_{b,i}$ are separately conserved at each site. Below we assume a uniform particle distribution $n_i = n$.

Equation (1) can be mapped into a Heisenberg-like spin Hamiltonian by defining the SU(2) local spin operators $\hat{L}_{+,i} = \hat{a}_i^\dagger \hat{b}_i$, $\hat{L}_{z,i} = (\hat{n}_{a,i} - \hat{n}_{b,i})/2$ [1,9]. Neglecting insignificant c-numbers, H_0 and H_c become

$$H_0 = \sum_i \left(-K\hat{L}_{x,i} + U\hat{L}_{z,i}^2 \right), \quad (4)$$

$$H_c = \mathcal{U} \sum_{\langle ij \rangle} \hat{L}_{z,i}\hat{L}_{z,j}, \quad (5)$$

where $\mathcal{U} = \mathcal{U}_{aa} - \mathcal{U}_{ab}$. Since $[\hat{L}^2, H] = 0$, the local spin magnitude is conserved at $\ell = \frac{n}{2}$.

III. MANY-BODY QUANTUM DYNAMICS

Normalizing the spin operators as $\hat{\mathbf{s}} \equiv \hat{\mathbf{L}}/\ell$, the Heisenberg equations of motion are given by

$$\frac{d}{d\tau}\hat{s}_{x,i} = -\frac{u}{2}(\hat{s}_{y,i}\hat{s}_{z,i} + \hat{s}_{z,i}\hat{s}_{y,i}) - v\sum_{\langle j \rangle} \hat{s}_{z,j}\hat{s}_{y,i}, \quad (6)$$

$$\frac{d}{d\tau}\hat{s}_{y,i} = \hat{s}_{z,i} + \frac{u}{2}(\hat{s}_{x,i}\hat{s}_{z,i} + \hat{s}_{z,i}\hat{s}_{x,i}) + v\sum_{\langle j \rangle} \hat{s}_{z,j}\hat{s}_{x,i}, \quad (7)$$

$$\frac{d}{d\tau}\hat{s}_{z,i} = -\hat{s}_{y,i}, \quad (8)$$

where $\langle j \rangle$ denotes summation over the nearest neighbors to site i. The dimensionless time in Eqs. (6)–(8) is $\tau = Kt$ and the dimensionless interaction parameters are $u \equiv \frac{Un}{K}$, which determines the internal Hilbert space structure of the individual dimers, and $v \equiv \frac{\mathcal{U}n}{2K} \ll u$, which dictates the energy exchange between neighboring dimers.

An exact many-body solution of the array's quantum dynamics can be obtained by either solving the Heisenberg equations (6)–(8) for the time-dependent operators $\hat{\mathbf{s}}(t)$, or by adopting a Schrödinger picture and solving for the time-dependent many-body quantum state $|\Psi\rangle_t$. Provided that the initial state of the system can be factorized as the product of single-site n-particle dimer states, the factorization persists at all times due to the lack of intersite particle transfer:

$$|\Psi\rangle_t = \prod_i \left\{ \sum_{m_i=-\ell}^{\ell} c_{m_i}(t)|\ell, m_i\rangle \right\}, \quad (9)$$

where $c_{m_i}(t) = \langle \ell, m_i | \Psi \rangle_t$, and $|\ell, m_i\rangle$ are the joint eigenstates of $\hat{L}_i^2$ and $\hat{L}_{z,i}$. This greatly reduces the Hilbert space dimension compared with the system considered in Ref. [19], making a numerical calculation possible. Substituting the factorized ansatz of Eq. (9) into the Schrödinger equation, we obtain a set of coupled differential equations for the amplitudes,

$$i\frac{d}{dt}c_{m_i} = \frac{-K}{2}[\sqrt{(\ell - m_i)(\ell + m_i + 1)}c_{m_i+1} + \sqrt{(\ell + m_i)(\ell - m_i + 1)}c_{m_i-1}] + Um_i^2 c_{m_i} + \mathcal{U}\sum_{\langle j \rangle} \langle m_j \rangle m_i c_{m_i}, \quad (10)$$

where

$$\langle m_j \rangle \equiv \sum_{m_j=-\ell}^{\ell} |c_{m_j}|^2 m_j \quad (11)$$

amounts to interactions with neighboring sites. Solving the set of Eqs. (10) numerically, the per-particle dimer energy in each site can be calculated as

$$E_i = \left\langle \left(-K\hat{L}_{x,i} + U\hat{L}_{z,i}^2 \right) \right\rangle / n. \quad (12)$$

IV. CLASSICAL MEAN-FIELD DYNAMICS

The classical, mean-field limit of the many-body dynamics is attained as N is increased while keeping u and v fixed. In this limit, dynamics initiated with a coherent preparation in each site can be approximately restricted to the product of classical coherent states,

$$|\Psi\rangle_t = \prod_i |\theta_i(t), \varphi_i(t)\rangle, \quad (13)$$

where

$$|\theta_i, \varphi_i\rangle = \frac{1}{\sqrt{n!}}[\cos(\theta_i/2)a_i^\dagger + \sin(\theta_i/2)e^{i\varphi_i}b_i^\dagger]^n|\text{vac}\rangle = [1 + \tan^2(\theta_i/2)]^{-\ell} \times \sum_{m=-\ell}^{\ell} [\tan(\theta_i/2)e^{-i\varphi_i}]^{\ell-m} \binom{2\ell}{\ell - m}^{1/2} |\ell, m\rangle. \quad (14)$$

For such minimal uncertainty states, the second-order expectation values of the dynamical variables $\hat{s}_{\alpha,i}$ can be factorized as the product of their first-order expectation values, i.e., $\langle \hat{s}_{\alpha,i}\hat{s}_{\beta,j} \rangle \approx \langle \hat{s}_{\alpha,i} \rangle \langle \hat{s}_{\beta,j} \rangle$ with $1/n$ relative accuracy [9]. Thus, $\hbar = 2/n$ serves as an effective Planck constant for the convergence of the many-body theory to its classical

limit. For $\hbar \ll 1$, quantum fluctuations diminish and the quantum-mechanical operators in Eqs. (6)–(8) may be replaced by the real-number Bloch vector components $s_{x,i} = \langle \hat{s}_{x,i} \rangle = \sin\theta_i \cos\varphi_i$, $s_{y,i} = \langle \hat{s}_{y,i} \rangle = \sin\theta_i \sin\varphi_i$, and $s_{z,i} = \langle \hat{s}_{z,i} \rangle = \cos\theta_i$ with φ_i and $n\cos\theta_i$ corresponding to the relative phase and population imbalance in site i, respectively [9,24]. Consequently, the mean-field equations of motion take the form

$$\frac{ds_{x,i}}{d\tau} = -u s_{z,i} s_{y,i} - v \sum_{\langle j \rangle} s_{z,j} s_{y,i}, \tag{15}$$

$$\frac{ds_{y,i}}{d\tau} = s_{z,i} + u s_{z,i} s_{x,i} + v \sum_{\langle j \rangle} s_{z,j} s_{x,i}, \tag{16}$$

$$\frac{ds_{z,i}}{d\tau} = -s_{y,i}, \tag{17}$$

and the classical dimer excitation energy per particle in site i is given as

$$E_i = -\frac{K}{2}\left(s_{x,i} + \frac{u}{2} s_{z,i}^2\right). \tag{18}$$

The classical ground-state energy of each dimer is $E_{\min} = -K/2$, obtained at $\mathbf{s} = (1,0,0)$. The total internal excitation energy $\sum_i (E_i(t) - E_{\min}) = E$ is conserved to a very good approximation, because the intersite coupling is weak.

V. TRANSFORMATION TO THE EXCITATION BASIS

Following Ref. [13] we transform the dimer-array Hamiltonian to the excitation basis, starting with a Holstein-Primakoff transformation (HPT):

$$\hat{L}_{x,i} = \frac{n}{2} - \hat{A}_i^\dagger \hat{A}_i \equiv \frac{1}{2}(\hat{a}_i^\dagger \hat{b}_i + \hat{b}_i^\dagger \hat{a}_i), \tag{19}$$

$$\hat{L}_{x,i}^+ = \hat{L}_{z,i} - i\hat{L}_{y,i} = \sqrt{n - \hat{A}_i^\dagger \hat{A}_i}\,\hat{A}_i \equiv \tfrac{1}{2}(\hat{a}_i^\dagger + \hat{b}_i^\dagger)(\hat{a}_i - \hat{b}_i), \tag{20}$$

$$\hat{L}_{x,i}^- = \hat{L}_{z,i} + i\hat{L}_{y,i} = \hat{A}_i^\dagger \sqrt{n - \hat{A}_i^\dagger \hat{A}_i} \equiv \tfrac{1}{2}(\hat{a}_i^\dagger - \hat{b}_i^\dagger)(\hat{a}_i + \hat{b}_i), \tag{21}$$

where $\hat{A}_i$ is the intermode atom moving operator with $[\hat{A}_i, \hat{A}_i^\dagger]=1$ and $[\hat{A}_i, \hat{n}_i]=0$. The coupling-free Hamiltonian (2) is thus approximated as

$$H_0 = \sum_i \left[-K\frac{n}{2} + K\hat{A}_i^\dagger \hat{A}_i + \frac{Un}{4}(\hat{A}_i + \hat{A}_i^\dagger)^2 - \frac{U}{8}\left\{(\hat{A}_i + \hat{A}_i^\dagger), \hat{A}_i^{\dagger 2}\hat{A}_i + \hat{A}_i^\dagger \hat{A}_i^2\right\}\right] + O(Un^{-1}). \tag{22}$$

The local Bogoliubov modes are then obtained by the usual transformation $\hat{c}_i = u_i \hat{A}_i - v_i \hat{A}_i^\dagger$, $\hat{c}_i^\dagger = u_i \hat{A}_i^\dagger - v_i \hat{A}_i$ with $[\hat{c}_i, \hat{c}_i^\dagger] = 1$ and choosing u_i and v_i so that the quadratic part of Eq. (22) is diagonalized. In the resulting expression, dropping the terms that do not conserve energy of the isolated dimer (i.e., terms not commuting with $\hat{c}_i^\dagger \hat{c}_i$), we get the coupling-free Hamiltonian in the Bogoliubov basis,

$$H_0 \approx \sum_i \left[-\frac{Kn}{2} + \omega_J \hat{c}_i^\dagger \hat{c}_i + U_J \hat{c}_i^\dagger \hat{c}_i^\dagger \hat{c}_i \hat{c}_i \right], \tag{23}$$

where $\omega_J = \sqrt{K(K+Un)}$ and $U_J = -\frac{U}{8}\frac{4K+Un}{K+Un}$ are the Josephson oscillation frequency and the effective strength of interaction between the Bogoliubov quasiparticles, respectively.

Using the same HPT equations (19)–(21), the interaction Hamiltonian (3) is transformed as

$$H_c = \frac{\mathcal{U}}{4} \sum_{\langle ij \rangle} \left[(\hat{A}_i^\dagger + \hat{A}_i)(\hat{A}_j^\dagger + \hat{A}_j)\left(n - \frac{\hat{A}_i^\dagger \hat{A}_i}{2} - \frac{\hat{A}_j^\dagger \hat{A}_j}{2}\right) + (\hat{A}_i^\dagger + \hat{A}_i)\frac{\hat{A}_j^\dagger}{2} + \frac{\hat{A}_i^\dagger}{2}(\hat{A}_j^\dagger + \hat{A}_j)\right]. \tag{24}$$

Performing the Bogoliubov transformation and retaining leading, energy-conserving terms, the coupling Hamiltonian representation in the excitation basis is

$$H_c \approx K_J \sum_{\langle ij \rangle} (\hat{c}_i^\dagger \hat{c}_j + \hat{c}_j^\dagger \hat{c}_i), \tag{25}$$

where $K_J = \frac{\mathcal{U}n}{4\sqrt{1+u}}$ is the effective hopping strength of quasiparticles between neighboring dimers. Thus, by contrast to Ref. [13] where the site coupling involved the transfer of particles, the coupling here corresponds predominantly to a linear exchange of excitations.

Considering Eqs. (23) and (25), the dimer-array Hamiltonian is effectively a BHH for attractively interacting excitations, with ω_J, K_J, and U_J functioning as self-energy, hopping, and interaction strength, respectively. This implies the possibility of obtaining discrete two-dimensional excitation solitons, similar to two-dimensional solitons in photonic lattices [22] and BECs [23]. The characteristic interaction parameter for the self-trapping of excitations should thus be

$$u_J = \frac{|U_J| n_J}{K_J} = \frac{u(4+u)}{4v\sqrt{1+u}}\frac{n_J}{n}, \tag{26}$$

where the approximate number of quasiparticles is deduced, by assuming equispaced low-energy excitations, to be $n_J \approx \sum_i \frac{n_i (E_i(0) - E_{\min})}{\omega_J}$.

VI. NUMERICAL SIMULATION RESULTS

To test for excitation self-trapping, we numerically simulate the dynamics of an extended 2D dimer array. Both classical (mean-field) and full quantum (many-body) calculations were carried out. The classical simulations were launched with $\{\theta_i, \varphi_i\}_{t=0}$ initial conditions that correspond to a single excited site, i.e., $E_j(0) - E_{\min} = E > 0$ and $E_i(0) = E_{\min}$ for all $i \neq j$. The many-body quantum simulations were similarly initiated with a direct product $|\Psi\rangle_{t=0} = \prod_i |\theta_i, \varphi_i\rangle$ of spin coherent states $|\theta_i, \varphi_i\rangle$ in each site, corresponding to the same relative phases and population imbalances. Such site-resolved state preparation and high-fidelity measurements have recently become experimentally feasible in a Hubbard-regime optical lattice [25].

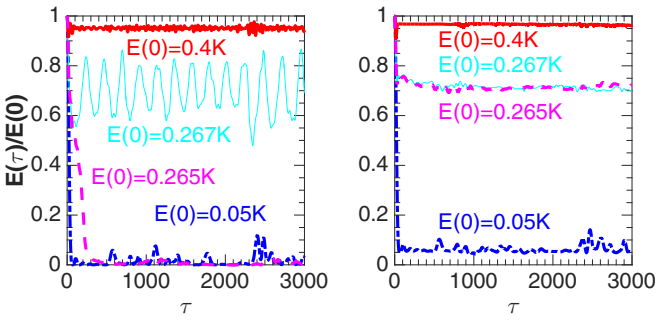

FIG. 1. Energy of the initially excited dimer site as a function of the rescaled time τ for various initial conditions. Mean-field results are plotted in the left panel, whereas full many-body calculations are shown on the right. Simulations were carried out with $n = 100$ particles in each site of a 20×20 array, with $u = 1.0$ and $v = 0.05$. The quantum initial preparations were coherent spin states $|\theta,\varphi\rangle$ corresponding to the same $\{\theta,\varphi\}$ as the classical preparations. Both calculations show self-trapping of excitations at high initial excitation energy vs dispersion at low excitation energy.

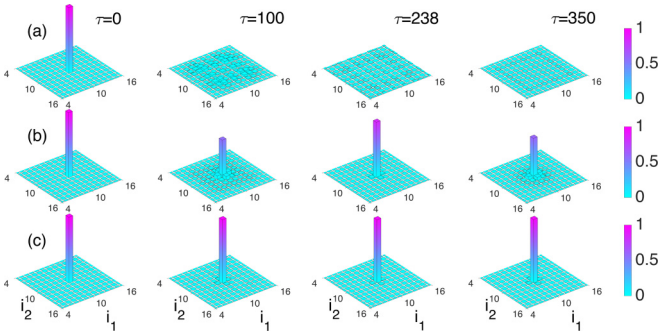

FIG. 2. Snapshots of the dimer excitation energy distribution in the array at different times during the classical evolution, for (a) $E/K = 0.05$, (b) $E/K = 0.267$, and (c) $E/K = 0.4$. When the initial excitation energy is small, energy disperses throughout the array, while larger initial excitation results in breathing and self-trapping. Parameters are as in Fig. 1. For clarity, only the central 13×13 sites in the array are shown. Energies are normalized to the initial excited dimer's energy in each case.

With n particles per site, each dimer has $(n+1)$ eigenstates and, considering the factorization (9), the total Hilbert space of the many-body system maps into $(n+1) \times M^2$ coefficients $c_{m_i}(t)$. Using a fourth-order Runge-Kutta method to numerically solve Eq. (10), exact many-body solutions can be obtained for a 20×20 array with $n = 100$ particles in each dimer site. In regions where the classical motion is stable, we expect this site population to give good quantum-classical correspondence (quantum break time scales as $\hbar \propto 1/n$). However, when the preparation lies in critical regions which contain dynamical instabilities, initially small quantum fluctuations grow exponentially, resulting in a weak $\log(n)$ growth of the quantum break time [9,26], and discrepancy between the mean-field and the quantum calculations is expected. This behavior is verified by the numerical calculations, as discussed below.

In Fig. 1, the energy of the excited site, starting at different initial values, is plotted as a function of time. When the initial excitation energy is low, it quickly disperses throughout the array. By contrast, higher excitation energies (a larger initial number of quasiparticles in the excited site) result in the self-trapping of energy with periodic exchange of excitations between the initially excited site and its close neighbors. Finally, for larger excitation energies, we obtain a stationary soliton of excitations.

While the classical transition from energy dispersion to self-trapping is very sharp, the corresponding quantum crossover is much more moderate. This is due to the finite uncertainty width of the quantum state, which results in the smearing of classical phase-space structures. While a single classical trajectory lies on either side of the separatrix and is thus either oscillatory or self-trapped, the quantum state may be viewed semiclassically as an ensemble of classical trajectories in phase space (as, e.g., in the truncated Wigner approach). As the initial quantum state crosses the separatrix, some of these trajectories become self-trapped while others remain oscillatory (as clearly seen in Fig. 3 below), thus broadening the transition. The width of the quantum transition region around the classical critical point is hence just the energy uncertainty of the initial quantum coherent state.

The evolution of the energy distribution in the array during the mean-field simulation for three typical initial conditions is plotted in Fig. 2. For small initial energy in the excited site, energy disperses rapidly through the array. However, beyond a critical value, the excitation energy remains self-trapped with breathing of the energy distribution. As the initial excitation energy is further increased, the breathing encompasses a narrower environment of the initially excited site, until a stationary two-dimensional energy soliton is obtained.

The classical phase-space trajectories $\mathbf{s}_i(t)$ in the initially excited site are presented in the upper panels of Fig. 3. Conservation of $\mathbf{s}^2$ implies classically that the norm s is conserved and the mean-field trajectories are restricted to the surface of the unit sphere, in accordance with the classical minimal-Gaussian ansatz of a pure state throughout the

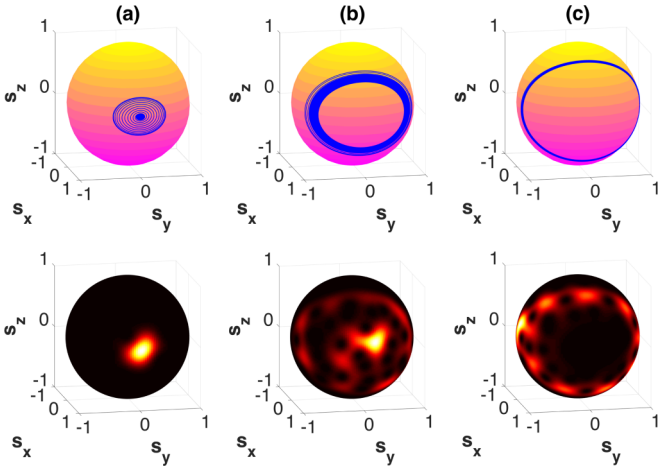

FIG. 3. Classical phase-space trajectories for the initially excited dimer (top) and the quantum Husimi phase-space distribution at $\tau = 400$ (bottom) for the same parameters as in Fig. 2.

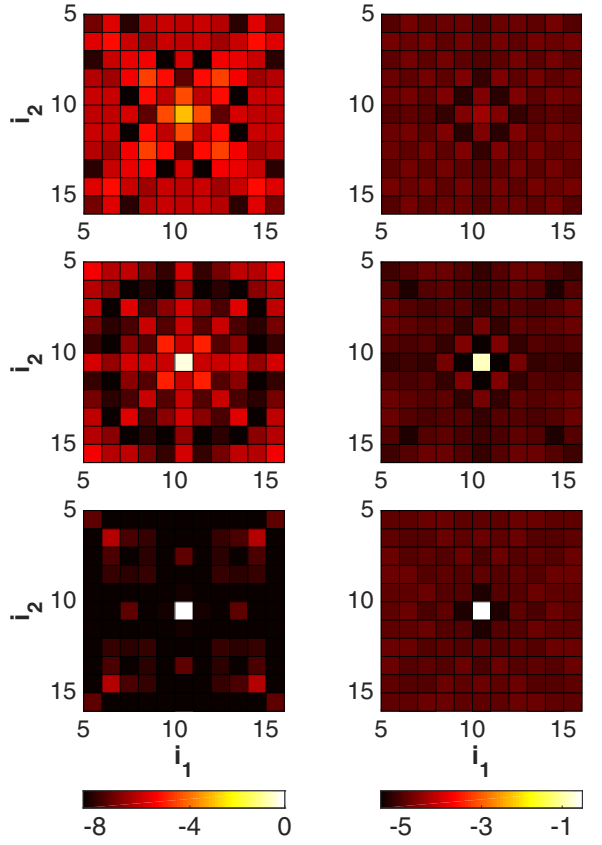

FIG. 4. Energy distribution $E_i(\tau)$ and one-particle entropy distribution $\mathcal{S}_i(\tau)$ at the end of the quantum simulation ($\tau = 3000$), for the same initial excitation energies and parameters as in Fig. 2. Note that the color map is scaled logarithmically. In order to clearly present the formed heat soliton, we focus only on the central 11×11 sites of the array.

evolution [9,24]. In agreement with the previous figures, a low-energy excitation decays to the classical ground state [$\mathbf{s} = (1,0,0)$], whereas higher excitations result in beating between two limiting excited trajectories and eventually full self-trapping on the initial energy contour.

The corresponding Husimi distribution $P(\theta,\varphi) = |\langle\theta,\varphi|\Psi\rangle|^2$ for the many-body quantum calculation at $\tau = 400$ is shown in the lower panels of Fig. 3. Unlike the classical case, conservation of $\langle\mathbf{s}^2\rangle$ does not imply constant $|\langle\mathbf{s}\rangle|$ due to the finite quantum variance of $\hat{\mathbf{s}}$ and the full quantum state loses its one-particle purity during the evolution [9,27,28]. If the relaxation to the coherent ground state is fast, the initial excited coherent state remains close to a minimal-uncertainty Gaussian and retains its one-particle purity. By contrast, when the excitation energy is self-trapped, the quantum phase-space distribution spreads all over the corresponding classical trajectory, and one-particle coherence is lost. This smearing suppresses the classical beating, as the distribution spreads to the entire region between the limiting energy contours rather than coherently propagating between them. For intermediate initial excitation energy, part of the initial coherent quantum distribution still has subcritical energy and hence decays, whereas the remaining part is self-trapped, resulting in a bimodal final

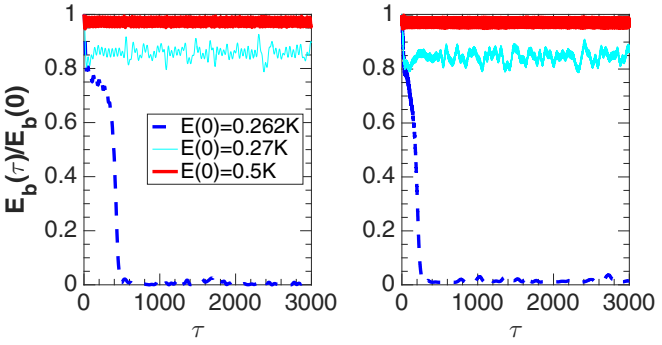

FIG. 5. Energy of the initially excited four dimer sites as a function of the rescaled time τ for various initial conditions. Mean-field results are plotted in the left panel, whereas full many-body calculations are shown on the right. Parameter values are chosen the same as in Fig. 1.

distribution (hence the gradual quantum transition from relaxation to self-trapping). The blurring of the classical features decreases with n as the size of the initial phase-space distribution becomes smaller and the mean-field limit is approached.

In Fig. 4 we plot the distribution of energy (left column) and of the entanglement entropy (right column),

$$\mathcal{S}_i = \mathrm{Tr}\left(\rho_i^{(sp)} \ln \rho_i^{(sp)}\right) = -\frac{1}{2} \ln\left(\frac{(1+s_i)^{1+s_i}(1-s_i)^{1-s_i}}{4}\right), \tag{27}$$

around the initially populated site, at the end of the propagation for the three representative excitation energies of the previous figures. Here, $\rho_i^{(sp)}$ is the reduced one-particle density matrix of the ith dimer. It is clear that, due to loss of one-particle coherence which accompanies self-trapping, the new localized structures are not only energy solitons but also entanglement-entropy solitons. In addition to being fundamentally important from a thermodynamical perspective, this feature may be useful for quantum-information-processing applications requiring quantum entanglement as a resource.

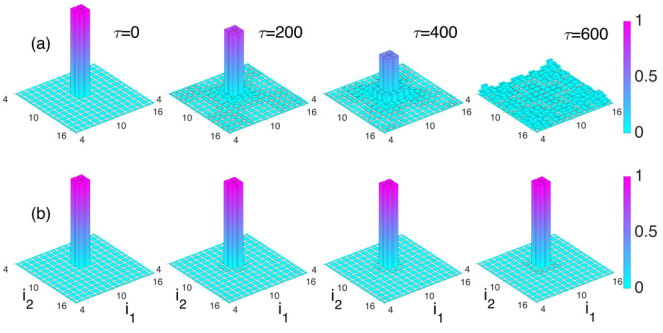

FIG. 6. Snapshots of the dimer excitation energy distribution in the array at different times during the classical evolution, for (a) $E/K = 0.262$ and (b) $E/K = 0.5$. When the initial excitation energy is small, the energy of the four sites disperses throughout the array, while larger initial excitation results in self-trapping. Parameters are as in Fig. 1. For clarity, only the central 14×14 sites in the array are shown. Energies are normalized to the initial excited dimer's energy in each case.

VII. DYNAMICS OF INITIALLY EXCITED BLOCK OF SITES

Before closing, we present the nature of energy dynamics when a block of sites is excited with equal energy E rather than the single-site excitation of the previous sections. Similar to Fig. 1, Fig. 5 shows a trapping of energy within a four-site block above certain initial excitation energy. We define the initial energy of the block by $E_b(0) = \sum_j^{\text{excited}}(E_j(0) - E_{\min})$ with $\sum_j^{\text{excited}}$ summing over the excited sites only. Here, the critical single-site excitation slightly differs compared to that in Sec. VI as the Bogoliubov quasiparticles on the adjacent sites affect each other. This minor difference in the critical excitation energy is due to very small density-dependent quasiparticle tunneling terms, which were neglected in Eq. (25). Figure 6 describes the energy distribution over the lattice at different times and features excitation trapping and relaxation at different initial energies of the block. Identical behavior was obtained for a block of 3×3 excited sites.

VIII. CONCLUSIONS

To conclude, using a two-dimensional array of Bose-Hubbard dimers with a weak nearest-neighbor interaction, we have demonstrated the macroscopic self-trapping of energy, with Josephson quasiparticles replacing the atoms of the standard schemes. The localization of excitation indicates a transition from ergodic to nonergodic behavior of the system [29,30]. In the self-trapped phase the excited sites do not relax and the long-time quantum state is strongly dependent on the initial out-of-equilibrium preparation. The resulting quasiparticle solitons feature localization of both energy and entropy, while the particle density is uniform. The existence of robust many-body states that do not dissipate in experimentally realizable settings would be helpful in designing experiments related to lossless quantum-mechanical architectures and hysteresis-based quantum memories [31,32].

[1] G. J. Milburn, J. Corney, E. M. Wright, and D. F. Walls, Phys. Rev. A **55**, 4318 (1997).
[2] S. Levy, E. Lahoud, I. Shomroni, and J. Steinhauer, Nature (London) **449**, 579 (2007).
[3] A. Smerzi, S. Fantoni, S. Giovanazzi, and S. R. Shenoy, Phys. Rev. Lett. **79**, 4950 (1997).
[4] S. Raghavan, A. Smerzi, S. Fantoni, and S. R. Shenoy, Phys. Rev. A **59**, 620 (1999).
[5] M. Albiez, R. Gati, J. Fölling, S. Hunsmann, M. Cristiani, and M. K. Oberthaler, Phys. Rev. Lett. **95**, 010402 (2005).
[6] M. Abbarchi, A. Amo, V. G. Sala, D. D. Solnyshkov, H. Flayac, L. Ferrier, I. Sagnes, E. Galopin, A. Lematitre, G. Malpuech, and J. Bloch, Nat. Phys. **9**, 275 (2013).
[7] R. W. Simmonds, A. Marchenkov, E. Hoskinson, J. C. Davis, and R. E. Packard, Nature (London) **412**, 55 (2001).
[8] R. Gati and M. K. Oberthaler, J. Phys. B **45**, 61(R) (2007).
[9] A. Vardi and J. R. Anglin, Phys. Rev. Lett. **86**, 568 (2001).
[10] I. Bloch, Nat. Phys. **1**, 23 (2005).
[11] T. Zibold, E. Nicklas, C. Gross, and M. K. Oberthaler, Phys. Rev. Lett. **105**, 204101 (2010).
[12] C. S. Gerving, T. M. Hoang, B. J. Land, M. Anquez, C. D. Hamley, and M. S. Chapman, Nat. Commun. **3**, 1169 (2012).
[13] M. P. Strzys and J. R. Anglin, Phys. Rev. A **81**, 043616 (2010).
[14] M. P. Strzys and J. R. Anglin, Phys. Rev. A **85**, 053610 (2012).
[15] M. P. Strzys and J. R. Anglin, Phys. Scr. **T151**, 014046 (2012).
[16] C. V. Chianca and M. K. Olsen, Phys. Rev. A **83**, 043607 (2011).
[17] C. Khripkov, C. Piermarocchi, and A. Vardi, Phys. Rev. B **88**, 235305 (2013).
[18] C. Khripkov and A. Vardi, Phys. Rev. A **89**, 053629 (2014).
[19] M. P. Strzys and J. R. Anglin, New J. Phys. **16**, 013013 (2014).
[20] F. S. Cattaliotti, S. Burger, C. Fort, P. Maddaloni, F. Minardi, A. Trombettoni, A. Smerzi, and M. Inguscio, Science **293**, 843 (2001).
[21] O. Dutta, M. Gajda, P. Hauke, M. Lewenstein, D. S. Lühman, B. A. Malomed, T. Sowinski, and J. Zakrzewski, Rep. Prog. Phys. **78**, 066001 (2015).
[22] J. W. Fleischer, M. Segev, N. K. Efremedis, and D. N. Christodoulides, Nature (London) **422**, 147 (2003).
[23] G. Gligoric, A. Maluckov, M. Stepic, L. Hadzievski, and B. A. Malomed, Phys. Rev. A **81**, 013633 (2010).
[24] M. Chuchem, K. Smith-Mannschott, M. Hiller, T. Kottos, A. Vardi, and D. Cohen, Phys. Rev. A **82**, 053617 (2010).
[25] W. S. Bakr, J. I. Gillen, A. Peng, S. Fölling, and M. Greiner, Nature (London) **462**, 74 (2009).
[26] J. R. Anglin and A. Vardi, Phys. Rev. A **64**, 013605 (2001).
[27] A. Imamoglu, M. Lewenstein, and L. You, Phys. Rev. Lett. **78**, 2511 (1997).
[28] E. M. Wright, T. Wong, M. J. Collett, S. M. Tan, and D. F. Walls, Phys. Rev. A **56**, 591 (1997).
[29] A. Pal and D. A. Huse, Phys. Rev. B **82**, 174411 (2010).
[30] A. Polkovnikov, K. Sengupta, A. Silva, and M. Vengalattore, Rev. Mod. Phys. **83**, 863 (2011).
[31] A. Trenkwalder, G. Spagnolli, G. Semeghini, S. Coop, M. Landini, P. Castilho, L. Pezzè, G. Modugno, M. Inguscio, A. Smerzi, and M. Fattori, Nat. Phys. **12**, 826 (2016).
[32] S. Eckel, J. G. Lee, F. Jendrzejewski, N Murray, C. W. Clark, C. J. Lobb, W. D. Phillips, M. Edwards, and G. K. Campbell, Nature (London) **506**, 200 (2014).